Dexterous robotic sampling for Mars *in-situ* science

P. S. Schenker, E. T. Baumgartner, S. Lee, H. Aghazarian, M. S. Garrett, R. A. Lindemann, D. K. Brown, Y. Bar-Cohen, S. S. Lih, B. Joffe, and S. S. Kim, Jet Propulsion Laboratory; B. H. Hoffman, Massachusetts Institute of Technology; T. Huntsberger, Univ. of So. Carolina

Jet Propulsion Laboratory, California Institute of Technology
4800 Oak Grove Drive/MS 125-224
Pasadena, California 91109-8099
paul.s.schenker@jpl.nasa.gov

ABSTRACT

Robotic exploration of the Martian surface will provide important scientific data on planetary climate, life history, and geologic resources. In particular, robotic arms will assist in the detailed visual inspection, instrumented analysis, extraction, and earth return of soil and rock samples. To this end, we are developing new robotic manipulation concepts for use on landers and rovers, wherein mass, volume, power and the ambient Mars environment are significant design constraints. Our earlier work led to *MarsArmI,* a 2.2 meter, 3-d.o.f. hybrid metal/composite, DC-motor actuated arm operating under coordinated joint-space control; NASA's Mars Surveyor '98 mission utilizes this design concept. More recently, we have conceived and implemented new, all-composite, very light robot arms: *MarsArmII,* a 4.0 kilogram, 2.3 meter arm for lander operations, and *MicroArm-1* and *MicroArm-2*, two smaller 1.0+ kilogram, .7 meter rover arms for mobile sample acquisition and Mars sample return processing. Features of these arms include our creation of new 3D machined composites for critical load-bearing parts; actuation by high-torque density ultrasonic motors; and, visually-designated inverse kinematics positioning with contact force adaptation under a novel task-level, dexterous controls paradigm. Our demonstrated results include robotic trenching, sample grasp-manipulation-and-transfer, and fresh rock surface exposure-probing via the science operator's "point-and-shoot" visual task designation in a stereo workspace. Sensor-referenced control capabilities include real-time adaptation to positioning error and environmental uncertainties (e.g., variable soil resistance and impediments), and the synthesis of power optimal trajectories for free space manipulation.

Keywords: space robotics, manipulators, intelligent control, mobile robots, planetary sampling, Mars sample return

1. INTRODUCTION

NASA's recent Mars Pathfinder (MPF) mission demonstrates the important role small rovers [32] can play in planetary science. Future, longer-ranging rovers will enable wide-area imaging/selection of science sites, analysis of surface terrain and outcroppings, collection of soil and rock samples, local meteorology, and many other functions -- including pick-up of cached samples for Earth return processing by an ascent vehicle. Similarly, the lander-based '98 NASA Mars Volatiles and Climate Surveyor [22] mission will probe southern polar extremities, using a robot arm to trench and closely view near-surface regolith samples, transferring same to lander onboard science instrumentation for further detailed chemical analysis. Such planetary exploration is fundamental to understanding the Martian geology, mineralogy, and climate; a possible life history; and, potential for a later human habitation.

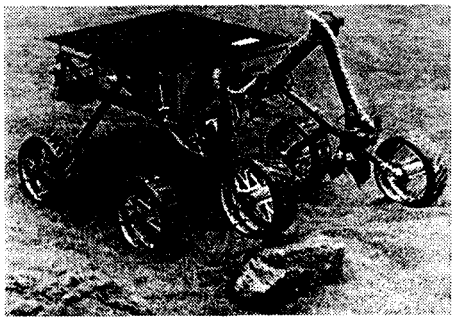

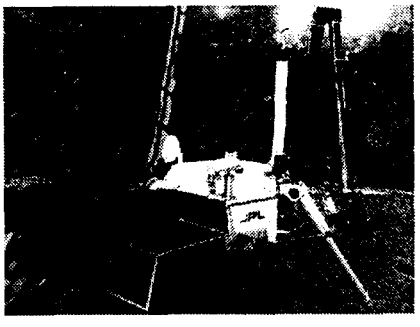

Figure 1. At left, the JPL *LSR-1* [25] rover with instrumented *MicroArm1*; at right, simulated Mars Surveyor '98 lander with *MarsArmII*. Both robot arms are all-composite construction and actuated by rotary piezoelectric motors. The rover arm at left is about 1:4 in scale/mass of the 4.0 Kg, 2+ meter lander arm at right; each carries a multifunction powered effector.

New robotic technologies are needed consistent with prevailing launch vehicle options (payload mass/volume), proposed science functions, intended science sites and duration of exploration, and the inherent long time delay and narrowband channels of deep space control & communication [32]. Further major design considerations include onboard computation and power resources. In **Figure 2** below, we summarize some work we are conducting toward development of light robotic arms responsive to future space mission requirements. We also discuss our related work on lightweight rovers in a companion paper of this meeting [25].

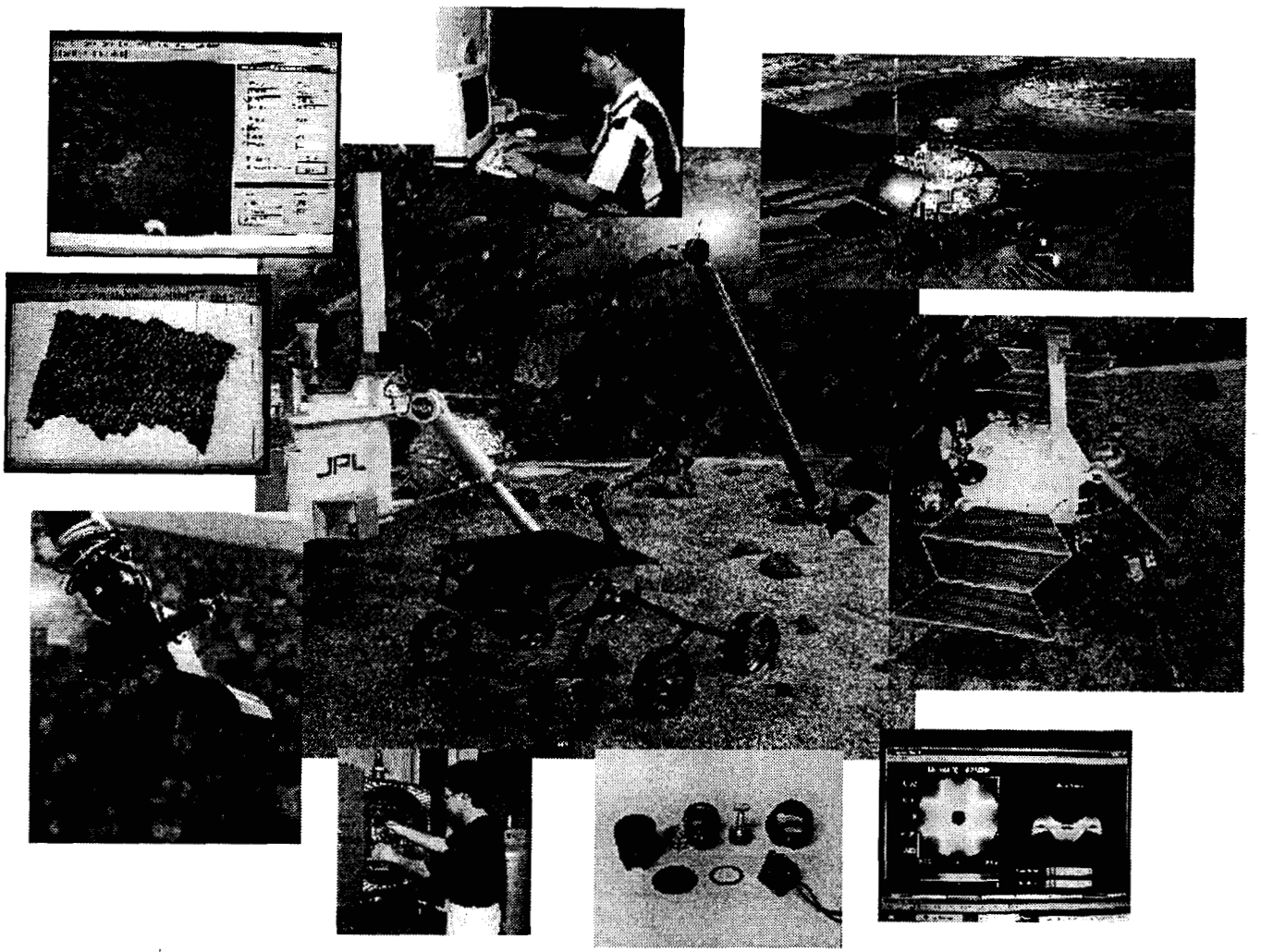

Figure 2. From upper left, counter-clockwise, around central figure of the lander-mounted MarsArmII and LSR-mounted smaller MicroArm-1 (in an early developmental stage): A science user interface for visually designating/selecting a particular task action (e.g., "trench along this line & angle, grasp this designated object, locate the arm camera here, etc."). A pseudo-color rendition of the 3-D terrain profile in the arm's workspace, as acquired by lander or rover-mounted stereo cameras. MarsArmII *MFSEE* (multi-function science end-effector), an all-composite 1 Kg "hand" incorporating clamshell gripper, integrated micro-camera, and active abrader for rock surface exposures (removal of weathering rind). Thermal testing of a low mass, high-torque density rotary ultrasonic motor for which PID servo and closed loop inverse kinematics positioning controls were developed. MarsArmII joint assembly showing such an actuator, in conjunction with machined 3D composite parts. Screen display of a JPL/MIT finite element analysis tool for prediction of motor properties, essential to design of servo controls and underlying drive electronics. *MarsArmI*, an earlier hybrid 2D composite-link/aluminum-joint robot prototype [23], performing simulated science operations; the MarsArmI design concept is being utilized in NASA's Mars Surveyor '98 science operations (ref: *Mars Volatiles and Climate Surveyor*; PI, Professor David A. Paige/UCLA), which, per upper right include searching for near ground ice by digging a trench, closely viewing stratigraphy of same with a robot arm camera, and transferring samples to thermal and evolved gas analysis (TEGA)

The primary foci of our work on new space robotic manipulation system concepts is threefold:

- creation of break-through low mass robot designs consistent with volume and power limitations of anticipated Mars missions, specifically the planned Mars Surveyor mission set ranging from Mars'98 lander science (*MVACS*) to Mars'01/'03 long range mobile science and sample collection, and a first Earth sample return circa '05. As one point of reference, the Mars'98 mission targets a 20 Kg, 70 liter, 25 Watt integrated science payload, with the arm itself on the order of 5 Kg and 10 liters stowage. Later Mars missions may afford as little as 5 Kg to integrated rover platforms, including arm mechanization, and there is comparable need in terrestrial field operations for light, agile vehicles, e.g., military scout and urban surveillance functions.
- coupled to appropriate mechanical designs, the development of autonomous sensing and control concepts sufficient to carry out unattended robotic science, compensating for modeled, and as possible, unmodeled system and environmental uncertainty. Some issues common to terrestrial/field robotics include positioning inaccuracies due to kinematics modeling error, limited visual resolution and eye-to-hand calibration of the visual workspace, guarded and force contact with unpredictable soft media and hard rock structures, and planning of arm/rover interactions and sensor assets during mobile science scenarios
- innovation of new materials, actuators, and mechanical designs suited to rigors of low ambient temperatures and atmosphere (< -100°C, 7-9 Torr CO_2), and associated wide-ranging diurnal cycles (> 100 °C)

In this paper, we emphasize the first two areas above; we recently reported on the third with regard to composite materials and ultrasonic motor development in reference [24]. Also, see our related work [25] with regard to development of integrated thermal-structural design for rover systems. In Section 2, we summarize features of the MarsArmII lander-based robot and the two smaller rover-based robots, MicroArm-1 and MicroArm-2, summarizing in each case the mechanical architectures and operating scenarios. In Section 3, we overview our ongoing development of task-level robot control and system/environmental uncertainty management during sampling operations; this presentation includes brief discussion of the *GOBS* (Goal Oriented Behavior Synthesis) construct; our multi-level sensor fusion and adaptive control architecture for robotic sampling, and within it, an approach to "self-calibrating" stereo. In Section 4 we report on a lower-level control strategy for minimizing robot arm power utilization during large free space trajectories; this concept seeks optimal use of constrained lander/rover energy resources during off-peak solar/thermal hours.

2. ROBOT ARMS AND OPERATING SCENARIOS

In this section we describe the lightweight serial manipulator concepts we have developed in support of various lander and rover sampling scenarios. All these developments are motivated by similar requirements to achieve reasonable positional dexterity and science function with minimal mass, volume, power impact to an integrated science payload. While the technical impetus and results of our work are general, the applications focus toward upcoming missions of the NASA Mars Surveyor Program (MSP) referenced above. Recent MSP lander configurations suggest the use of ~2 meter/5-10 Kg/20-30 W robot arm solutions. MSP rover configurations are still being defined, and given their broad scale of applications (5-to-10 Kg fast sample cache return up to 20-50 Kg long range science) admit many possibilities for arms and integrated tools [30]; current rover concepts suggest arms of .5-1 m/1-4 Kg/5-10+ W. The actual functions and instrumentation of a given arm are determined by request/requirement of science users, and any mission logistics by which an arm would perform basic "facility" inspection,/housekeeping. The intent to date of equipping landers and rovers with arms is *sample acquisition*, harking back to NASA Viking lander operations of the mid-'70's. Basic sample acquisition comprises picking up surface/near-surface materials of interest for onboard science analysis and/or taking preferred miniature instrumentation to selected samples. Included in this function are close-up viewing, scanning, and probing modalities of interaction with the surface (including its atmospheric boundary layer), e.g., by means of arm-borne cameras, point spectrometers, multispectral imagers, meteorology stations, spectroscopes (Moessbauer, APXS, Raman, other). In many cases, materials of interest – accumulated surface layer (regolith), small rocks, and trenched examples of same – are useful in native form. However, it may be desirable to expose/extract fresh rock materials, removing any weathering rind features and dust contaminants so as to providing a pristine surface or core sample for chemical assay. This imposes additional robotic requirements in the form of coring/drilling/chipping/ablation functions, whether by arm-carried tools or dedicated mechanisms. A complementary function to sample acquisition is *sample caching & containment.* The defined scope of this activity is archival storage (a "cache") of materials obtained during sample acquisition, and the sequence of sample cache pick-up, transport, and materials processing to guarantee planetary protection ("containment") in an Earth return phase of the mission. One scenario, in the context of MSP '01-'05 options, would have long range science rovers [10]: 1) traveling 10's of Km, selecting-acquiring-caching samples of interest, 2) taking cached materials to a central repository or retaining them onboard (the "dead" rover or depository position would be noted, with a beacon left operative), and 3) subsequent "Mars Sample Return" precision landing, rendevous and pick-up by fast cache retrieval rover [25], and transport to ascent vehicle processing. Containment might occur in both steps 2 and 3, with the latter most likely.

2.1 MarsArmII

MarsArmII is a second generation lander-based serial manipulator of 2 meter, 5 kilogram (with 1 Kg effector), 25 Watts (earth simulation) class. The arm, given space operations scenarios, is not designed to move quickly; but, within this constraint, it is still desired to make the arm as stiff as possible to minimize self-deflections and deflection under applied environmental load. The approximate first mode of vibration of the arm, per design parameters below, is estimated at 7 Hz. The maximum self-weight deflection of the arm end-point outstretched on Earth is about .25 inches, while on Mars (.39 g) the deflection would be .10 inches, as accumulates from deflection in the tubes and joints. The principal technology demonstration goals are to advance hybrid metal-joint and 2D composite-link, DC-actuated arm design of MarsArmI [23] into 30-40% lighter all-composite construction, evaluating also use of rotary ultrasonic motors (USM's [29]) as arm actuators. We describe these materials and actuation components of MarsArmII design in detail in reference [24]; we discuss related progress in all-composite lightweight rover design in [25]. All-composite robot construction has been possible through our development of a new 3D randomized air lay-up carbon fiber resin transfer mold (RTM) process; this technology yields cured billets which can be machined-drilled-and-tapped to intricate parts. Not only is this 3D composite a strong, light material for critical load-bearing assemblies such as robot joints; it also potentially enables better thermal tuning of mechanical stresses which develop due to CTE mismatch at metal-composite and metal-to-metal interfaces (cf. aforementioned 100+ °C diurnal swings on Mars, and issues of mechanical survivability in extended duration missions). Regarding actuation, USMs have advantages of self braking (non-backdrivability), inherently low operating speeds at high torques, and 3-10x torque density of conventional DC motor designs. This facilitates reduced gearing mass and makes USMs very attractive for robotic actuation, e.g., joints, effectors, and rover wheel assemblies. USMs developed to date have been targeted at room temperature and earth ambient (1 ATM) consumer electronics applications utilizing simple if any closed loop servo control. We are developing new USM designs having reverse segmented and stacked piezoelectric drivers (compare to conventional poled crystal designs) which are expected to be tolerant of low temperature operation and thermal cycling; our related experimental work includes characterizing motor performance and design parameters under salient Mars operating conditions (as to material, structural, and electrical issues, e.g., DTCE effect on close-tolerance mechanical/electrical interfaces, and discharge-arcing-breakdown phenomena in reduced atmospheres). In physical principle, USM's are operable to near 0°K. In experiments to date, we have successfully operated test devices for 10's of hours at 120°K and near cryo-vacuum conditions; these initial trials include some thermal cycling analysis.

MarsArmII, pictured in Figure 2 above, is a two link serial arm with 4 d.o.f. having a single d.o.f. end-effector with opposable thumb scoop in modified clamshell configuration. The end-effector also carries an integral micro-camera and active abrader, respectively for use in close-up geological analysis and powered exposure of fresh rock surfaces (removing oxidized weathering rind). The kinematics arrangement of the arm is a torso-shoulder-elbow-wrist. The torso and shoulder joints connect in series at the base with link 1 connecting to the shoulder joint output. At the end of link 1 the stator side of the elbow joint is connected. At the output or rotor side of the elbow joint is the connection to link 2. The end of link 2 connects to the stator side of the wrist joint, and the rotor side of the wrist joint connects to the end effector housing. The full extent length of MarsArmII is 90 inches or 2.3 meters. MarsArm II is configured as a RRRR robot arm with an additional degree of freedom which is used to open and close the end-effector scoop. The forward kinematics of this arm can be described in standard Denavit-Hartenberg (D-H parameters):

Joint(i)	alpha(i-1)	a(i-1)	d(i)	theta(i)
1	0	0	0	theta(1)
2	-90 deg	a1	d2	theta(2)
3	0	a2	d3	theta(3)
4	0	a3	d4	theta(4)

where a1 = 4 inches, a2 = 44 inches, a3 = 43.895 inches, d2 = 3 inches, d3 = 3 inches, and d4 = 2 inches. Note that the tip position and orientation of the end-effector can also be determined via the forward kinematics through knowledge of the scoop length and the opening angle of the scoop (theta(5)).

The inverse kinematics of MarsArm II have also been determined and are used to compute the joint configuration that achieves a given end-effector position as well as a given in-plane orientation of the end-effector. In general, given the desired end-effector location, the roll joint (theta(1)) is first computed. Once theta(1) is determined, the remainder of the arm can be considered to be a planar arm which maneuvers in what we call the "trenching plane." Then, given the end-effector tip position with respect to the trenching plane and the end-effector orientation also with respect to the trenching plane, the last three joint rotations (theta(2) -

theta(4)) are calculated. During baseline robotic operations, a stereo camera pair (mounted on the lander base) are calibrated such that they provide an accurate 3D map of the area in front of the lander base (see example of Figure 1 inset, middle left). This 3D map has been determined to be accurate within several cm. Therefore, given a desired physical space location to approach (selected by the remote operator) and a given end-effector in-plane orientation, the joint configuration which achieves this pose can be determined through the inverse kinematics.

As discussed further below, the arm links are graphite epoxy tubes 40 inches long. The tubes have an outer diameter of 2.5 inches and their wall thickness is 0.040 inches. The graphite epoxy tubes are made of 8 layers of unidirectional fibers in a hand wrapped lay up. The tubes weigh .692 lb apiece. Bonded into the ends of the tubes are reinforcing end caps made of Aluminum 6061-T6 (similar 3D composite parts under evaluation). Each tube has bonded to it near the base a semiconductor force sensor pair used to measure the output torque of the joint for use in explicit force control, which is another novel arm feature. The mass of each tube with end caps, and force sensors is 1 lb.

The first three joints of the arm are identical. They utilize a Shinsei (Litton-Westrex, Inc.) USR60S1 ultrasonic motor (USM), that has been experimentally determined to deliver about 4.5 in-lb of torque at stall with an unloaded maximum speed of 100 rpm. The USM's are equipped with a relative optical encoder resolving 500 pulses per shaft revolution. The USMs input to a harmonic drive having reduction of 160:1. The harmonic drives used are CSF-20-160's provided by Harmonic Systems, Inc. This gives an output stall torque capability for the joints of ~500 in-lb assuming a typical 70% total efficiency. The output side of each joint is held by two Kaydon, Inc. "Really Slim" angular contact bearings with an inner diameter of 2.5 inches. In addition a potentiometer is included internal to the joint as an absolute position device. The potentiometer is a 10 turn rotary coil type. Reduction gearing of the output side of each joint enables the potentiometer to make 4 revolutions for each revolution of the output joint, thus increasing resolution of the potentiometer measurement. These actuation components are structurally integrated within an joint assembly made of 3D machined composite parts noted above. The fully integrated joints, 1-3, cumulatively weigh 2.5 lb.

The end-of-arm wrist joint is a different design, which also serves as basis for the three primary arm joints of the rover-mounted MicroArm-1 depicted in Figure 1. The wrist joint utilizes a 1 in-lb Shinsei USR30E3 USM with a no load speed of 300 rpm and an integral optical relative encoder. The 1 in-lb USM inputs to a CSF-14-100 harmonic drive with a reduction of 100:1. The output torque of the wrist joint is approximately 65 in-lb after all of the mechanical losses. The output side of the wrist joint utilizes a single Kaydon "Really Slim" ball bearing with a bore of 1.5 inches. The single bearing is of the x-Type which means it is capable of supporting significant moment loads. The fully assembled wrist joint weighs .7 lb.

Finally, the arm end effector (per lower left inset of Figure 2) also utilizes the 4.5 in-lb Shinsei USM of the MarsArmII primary joints, but with a 10:1 worm screw and two worm gears to power each opposing clamshell digit. The worm gears are mounted on either side of the worm screw. The worm gears are on parallel shafts with a Berg, Inc. ball bearing at the end of each shaft. Given an 80% efficiency of the gearing, the end effector digits share 36 in-lb of torque, powering a 5 inch long scoop and thumb. The maximum speed of the end effector tip as driven by the torso or shoulder joint is about 5.7 inches/sec, and the lowest speed is .577 inches. The arm is designed to provide a tip force capability of 8 lb., or to carry up to 8 lb. of samples or instrumentation in its end effector. The end effector incorporates a simple grinding (Dremel-style) tool powered by a small DC brushed motor.

The real-time computer for our MarsArmII operations is VME 68040/VxWorks environment, interfaced to a programmable Galil, Inc., motor controller board (PID/joint trajectory), which in turn drives custom electronics of the ultrasonic motors. This lander system and its C-based program functions interact via BSD socket protocol and ethernet link with a nearby science operator visual user interface hosted on a Pentium PC (Windows95/Visual C++ routines). As illustrated in Figure 2 above, the lander mast carries a stereo camera pair enabling estimation of a 3D surface terrain map. The terrain map, given a prior calibration of lander camera models and robot workspace, enables the operator to designate image targets of interest (location, trench line/angle/depth) and invoke task-level "skills" such as trenching, acquisition, sample-transfer-and-deposition, viewing-probing, rock abrasion, etc. These skills are accessible as various menu pull-down functions of the operator interface with integrated visual display of the workspace, as shown in Figure 2 upper left. We discuss the task control and visual calibration functions further in Section 3.

2.2 MicroArm-1

MicroArm-1 is a .7 meter long, 1.5 Kg (with effector) robot arm for use on proposed rovers, and has a strong design and component heritage from MarsArmII. One of the basic objectives in creating MicroArm-1 -- basically a rapid prototyping exercise -- was to see if the new 3D composite and USM-based design concept would scale to smaller applications. The first three joints of MicroArm-1 are identical to the wrist joint of MarsArm II. These three joints connect to two graphite epoxy tubes that are 8.25

inches long. The kinematics configuration of MicroArm-1 is like that of MarsArm II. The MicroArm-2 wrist joint and end effector also employ 1in-lb Shinsei USMs, powering 20:1 Berg, Inc., reduction worm gearing sets. As in the end effector of MarsArmII, worm gears are mounted to twin parallel output shafts, as affixed on the either side of the worm screw which is mounted directly to the shaft of the USM. The twin output shafts have mounted at each end a Berg ball bearing which is set in a structure made from the 3D graphite epoxy material. The maximum tip speed of MicroArm-1 is 9.4 inches/sec, and the minimum is .94 inches/sec. The end effector of the is capable of lifting or applying 4 lbs of force. In design and function the end effector is similar to MarsArmII's MFSEE, carrying an identical DC powered abrasion tool, a micro-viewing color camera, and a scoop and with opposable thumb.

MicroArm-1, Figure 1 and close-up left, integrated with JPL's *Lightweight Survivable Rover* [ ] to demonstrate dexterous science manipulation functions. As with MarsArmII, these tasks are carried out under visually referenced, inverse kinematics control:

- close-up visual inspection of with end-effector mounted micro-camera
- miniaturized instrument emplacement and/or positional scans & probing
- sample acquisition and on-board storage (sample caching concept)
- trenching and digging of rover soils surrounding the rover
- sample manipulation including rock manipulation (flipping, turning, etc.) and transfer of rock to on-board science instrument/analysis
- fresh rock exposure using a simple end-effector mounted Dremel-type tool (initial feasibility study of hard force contact operations from compliant rover base)
- integrated force feedback operations for sample handling tasks

Figure 3. LSR-1 rear left view (MicroArm-1 replaces rear science tray) as equipped to perform sample acquisition, close-up viewing and fresh rock exposures

2.3 MicroArm-2

MicroArm-2 is a 3-d.o.f. serial manipulator with articulated end-effector -- similar in concept to MicroArm-1, but differing in kinematics and implementation. MicroArm-2 is driven by DC brushed motors and conventional closed-loop PID controllers using optical encoder feedback. Likewise, rotational position sensors are used in all joints to provide absolute joint rotation information.. The first demonstrated application of MicroArm-2 is sample cache retrieval from a science rover during simulated Mars sample return operations. As shown below, this scenario is being implemented on JPL's new *Sample Retrieval Rover* [25], a 5 Kg class, four-wheel bogie mobility platform (20 cm dia.) having fully collapsible running gear.

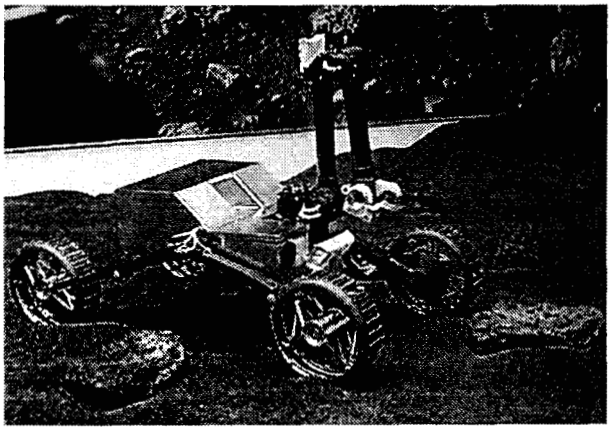

In addition its cache transfer function, MicroArm-2 carries at its elbow a goal recognition camera. This camera (with visual navigation and robot arm visual guidance being supported by a stereo pair) is used to acquire the science rover, providing heading and range estimates to the sample cache located on-board that rover (or any other recognizable feature set of areal interest, e.g., depository or even sample). Similar to MicroArm-1 and MarsArmII, the construction of MicroArm-2 is again based in 2D composite links and 3D machined composite joints. However, Micro-Arm-2 utilizes a composite process having higher fiber density, in more preferentially oriented carbon preform. Early mechanical tests indicate this new material will yield mass-equivalent components of greater strength than aerospace grade aluminum, while retaining the desirable CTE interface properties noted for the lower density 3D composite.

Figure 4. Sample Retrieval Rover in JPL Planetary Robotics Lab with front-mounted 3-d.o.f MicroArm-2 and talon-scoop end-effector for cache pick-up (goal acquisition camera at elbow, articulated axle vehicle in "squat pose")

The design of MicroArm-II is such that all links lie in a common plane, with offset at the elbow joint to provide for compact stowage on-board SRR. The articulated end-effector was designed for the specific task of gripping the cylindrical handle of the sample cache container. When the cylindrical handle is located between the actuated upper scoop of the end-effector and the fixed lower thumb, a three-point grip is realized. We confirm presence or absence of the handle within the end-effector via an IR emitter/ detector pair embedded in the housing of the fixed lower thumb. If the arm is correctly positioned such that the handle enters the gripper, then the IR beam is interrupted, verifying successful acquisition of the sample cache container.

MicroArm-2, as MarsArmII and MicroArm-1, derives workspace position coordinates primarily from 3D stereo information [13]. The rover platform carries a calibrated stereo camera pair, which more generally is utilized for navigational obstacle detection and avoidance, as well additional possible areal sensor fusion functions [21]. If a point of interest can be correlated in the stereo pair, then it is solvable for 3D coordinates relative to a proscribed base frame of the manipulator. This Cartesian information (whether in fact a simple point "marker," or more general feature localized in position-and-orientation in the base frame, e.g. the cache can handle) is in turn solvable for inverse arm kinematics to reach-and-acquire. With regards to this global eye-hand coordination function, we are developing -- within the *GOBS* task control architecture further discussed in Section 3 below -- means to directly feedback visual information of an end-effector feature to iteratively update the calibration, as well as more generally perform visual servo functions. This "self-calibrating stereo [16]" is particularly desirable in a space environment wherein significant thermal stresses and cycling effects may introduce unpredictable bias into prior calibrations. See also our related earlier work on visual position guidance in which a direct camera space model for eye-hand coordination can be derived [17].

The forward kinematics of MicroArm-2 can be described as a modified Denavit-Hartenberg representation:

Joint_i	alpha_(i-1)	a_(i-1)	d_i	theta_i	l_i
1	0 deg	0	0	theta_1	0
2	-90 deg	a_1	0	theta_2	0
3	0 deg	a_2	0	theta_3	l_3
W	0 deg	a_3	0	0	0
E	0 deg	a_E	0	0	l_E

This is not a standard D-H representation due to offset that occurs at the elbow joint (joint 3). The l_3 parameter takes care of this offset in the joint-local "y" direction. The "W" represents the center of the wrist housing. The "E" represents the end-effector location, which we define as the tip of the thumb -- the leading point on the arm as it enters the handle of the sample cache can. The numerical values for these parameters are given below left and the resultant end-effector position (X_E, Y_E, Z_E) at right :

a_1 = 2.725 in
a_2 = 11.225 in
a_3 = 10.05 in
l_3 = 2.4125 in
a_E = 0.16862 in
l_E = 1.71165 in

X_E = cos(theta_1)*[cos(theta_2+theta_3)*a_E - sin(theta_2+theta_3)*l_E +
cos(theta_2+theta_3)*a_3 + cos(theta_2)*a_2 - sin(theta_2)*l_3 + a_1]
Y_E = sin(theta_1)*[cos(theta_2+theta_3)*a_E - sin(theta_2+theta_3)*le +
cos(theta_2+theta_3)*a_3 + cos(theta_2)*a_2 - sin(theta_2)*l_3 + a_1]
Z_E =-sin(theta_2+theta_3)*a_E-cos(theta_2+theta_3)*l_E -
sin(theta_2+theta_3)*a_3-sin(theta_2)*a_2-cos(theta_2)*l_3

3. SENSOR-BASED CONTROLS FOR ROBOTIC SAMPLING

As we have outlined above, the Mars robotic manipulation tasks we perform fall into categorical areas: acquisition & trenching of soil, grasping and manipulating small rocks, performing instrumented scans of designated objects or areas-of-interest, emplacing and/or retrieving small instruments, and dexterous handling-transport-processing of containments. Such activities may include not only direct manipulation of Mars surface/sub-surface media, but also the acquisition, dexterous handling, stowage of powered tools or instruments whose kinematically and force-linked interactions with the environment are complex [13] (a core drill being applied at the end of arm to a rock, the near surface scan of an outcropping, etc.). Certainly the idealized performance is a "field geologist" human equivalent, if not the practical or achievable engineering solution. In the most aggressive scenarios, one can also imagine an arm as integral to vehicular terrain management, being used as a stabilizing support member, controllable c.g. element, or even to free a trapped vehicle. All these functions are inherently unstructured activities: while the science task objective, operational

sequence, and robotic control procedures can be planned in advance, there are sensing and control uncertainties that must be resolved shortly prior to task execution, or in real-time [2, 3, 5, 9, 19]. Conceptually simpler examples are maintaining accurate eye-to-hand calibration, obtaining good relative positioning under limited visual acuity, adapting robot arm force/position trajectories to unmodeled environmental properties, compensating arm control for platform disturbances/constraints (robot base compliance, power limitations, etc.) [6]. These examples are at lower levels of control abstraction, and in some cases amenable to a simple design trade, a mechanical work-around (a cooperative fixture, etc.), or good point design implementation.

However, at higher levels of control abstraction -- levels that cannot be "engineered out" with pre-programmed sequencing given lack of task structure -- there is the problem of synthesizing a small, practical set of autonomous sampling "skills," or discrete event dynamical system models that are behaviorally "robust." Our sense of the last word is both informal and literal. The casual meaning is to introduce sufficiently adaptive behaviors, at all control levels, so as to *autonomously* complete the task objective, in reasonable time, without compromise of system safety or science integrity. In a more specific, formal sense the meaning is to invoke higher level sensing and control procedures that are *optimal* – making maximally efficient use of sensor data (according to its modeled statistical content, data fusion/decision criterion, etc.), and realizing task control within minimal complexity (e.g, as characterized by control syntax, linguistic efficacy, etc.). These problems are relevant to both telerobotic and highly automated operations [5]. Our emphasis is toward the latter for planetary sampling due to inherently long time delays between uplinks/ downlinks, and the desire to maintain a high level of mission productivity during windows of optimal science activity and opportunity. Given these considerations, we are developing a multi-level, multi-rate sensor fusion and adaptive control architecture – a event-driven, statistical perception & action network computing paradigm -- called *Goal-Oriented Behavior Synthesis* (GOBS). Within this framework, we are currently implementing soil trenching and rock sampling procedures, also an approach to "self-calibrating" stereo. We first outline the continuous sensor-based controls used in of our lander and rover arms, then we summarize the GOBS concept, motivating same with an "adaptive trenching" example. See also our related presentations of *GOBS* decision-theoretic models, network synthesis, dynamical convergence properties, and simulation results in [15, 16].

The basic position controls operation of our lander and rover sampling arms is to specify a desired location in the workspace image, a 3D trajectory or grasp action at that site, and execute it under visually-referenced inverse kinematics control. We have developed verified kinematics models for our arms (more accurate than visual workspace resolution or its calibration); we utilize well-understood visual eye-to-hand calibration [13, 33] procedures (modeling the lander mast or rover stereo camera pair extrinsic and intrinsic parameters, some basic camera optical nonlinearities, and sampling robot world frame); finally, we have derived and implemented inverse kinematics solutions that execute accurately and reasonably quickly in on-board 32-bit real-time terrestrial computing environments (68040/80486). We have developed an empirical PID control of the rotary ultrasonic motors, and basic coordinated joint-level motion control for same, in both cases adapting the hardware programmable modes of a Galil, Inc., motor control board operating within a VME/VxWorks environment. Further understanding of these motors is sought, particularly a good dynamical model and optimal PID servo-control synthesis; our experimental work has given us useful insight into the motor behaviors under closed loop servo, but given this is a first principled use of such actuators in precision control, we as yet lack a sense of optimal gain tuning, etc. Within this experimental controls framework, we can, as one example, smoothly position the 2+ meter MarsArmII to several centimeters accuracy across the lander near-field terrain of Figure 2 (arm positioning accuracy is, of course contingent on stereo baseline and calibration, and the resolvable relative position control of the arm is far greater, on the order of mm or less for all our arms). Similarly, we can position our rover arms, per Figures 3 and 4 to several mm). In addition to such position controls, both MarsArmII and MicroArm-1 implement a conventional force-feedback compliance control, as derived from explicitly measured arm strains recorded by calibrated semiconductor gauges within arm links and effector assemblies.

3.1 *Goal-Oriented Behavior Synthesis* (GOBS), an approach to intelligent automation of robotic sampling

Robots engaged in planetary sampling require intelligence to cope with their structural and environmental ambiguities, as well as unexpected events that may induce faulty performance. Developing a sensor-based control architecture that computationally connects distributed sensors and actuators in such a way as to explicitly, iteratively reduce modeled uncertainties during real-time operation as well as detect, monitor, and sequentially repair system wide errors and faults is thus highly desirable [2, 3, 19]. The implementation of such robot intelligence requires integration of planning and control of events on multi-resolution time scales, ranging from continuous time control to discrete event planning [1, 3]. Conventional architectures for intelligent robotic systems do not address the problems of reducing uncertainties or dealing with unexpected events through error repair. Further, the general efficacy and efficiency of integrating planning and control in multi-resolution time scales towards robotic performance goals are yet to be well understood or comparative benchmarks established. The GOBS sensor-based construct seeks to formalize these problems in an extensible network architecture, one that is easily expanded, refined and made more robust with both the addition of physical network resources and improved representation of sensors, their feature transformations, and network constraints.

3.1.1. GOBS architecture.

GOBS consists of two major building blocks, the *perception net* and *action net* [15, 16]. The perception net, as illustrated in **Figure 5** for a soil science task, connects features or logical sensors [11] of various levels of abstraction that can be extracted by the sensor system. The novelty of the perception is that the features or logical sensors are interconnected with explicit description of their relationships in terms of feature transformation, data sensor fusion, and constraint satisfaction modules, such that the uncertainties associated with individual logical sensors can be explicitly propagated through the net [8]. Uncertainty of each logical sensor, represented as a hyper-ellipsoidal bound, is continuously updated by fusing sensor data and by constraints imposed on logical sensor values. The uncertainty propagation in the perception net serves as the basis of error detection and identification. See [16] for discussions of the actual uncertainty models, propagation constraints & logic, and network dynamics.

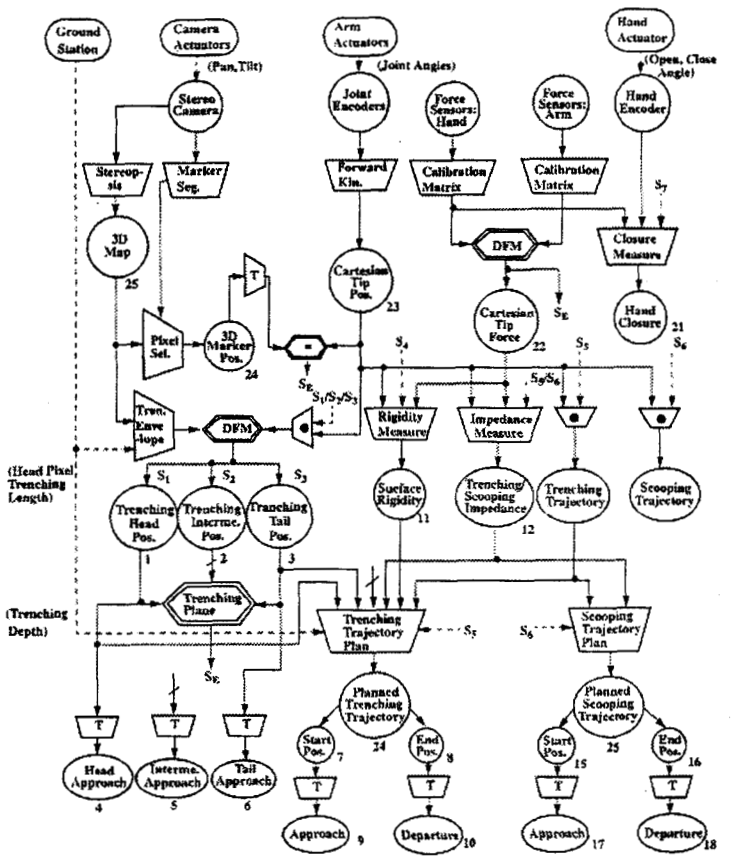

The action net consists of a hierarchy of state transition networks of multi-resolution time scales, representing both continuous time as well as discrete event system dynamics. The action net realizes a system dynamic model in a global sense, wherein all feasible system behaviors are embedded. A state transition network of smaller time scale implements an action defined on a larger time scale. This allows the system to replan behaviors towards set *goals* should errors, faults, or unexpected events occur, hence our terminology "goal-oriented behaviors (GOB)." There is a formalizable analogy to linguistics: a feasible system behavior generated by the action net in conjunction with the perception net (through planning and control) is equivalent to generating a sentence from a language in which a large number of sentences are embedded in its grammar and vocabularies. Through the perception net, GOBS explicitly manages uncertainties. Uncertainties associated with individual logical sensors (depicted as circle) are propagated through such functional modules as data fusion module (DFM), feature transformation module (FTM-trapezoid), and constraint satisfaction module (CSM-double hexagon). The values associated with logical sensors are updated through forward and backward process of reaching an equilibrium point. By way of example, the generalized reduction of uncertainty in locating the robot scoop at a designated trenching site is embedded in sensor fusion of the joint encoders, updated stereo calibration/visual servo with a robot marker, tactile exploration of scoop, as well as the proscribed trajectory constraint from the trenching plane.

Figure 5. Goal Oriented Behavior Synthesis perception network for robotic soil sampling system (trenching)

Note that the sensor fusion module and/or constraint satisfaction modules also support error detection and identification. For instance, errors can be detected when there exists excessive error between planned and measured states (represented by the perception net) or large inconsistency of data at a DFM or excessive violation of constraints at the a CSM. Then, based on the perception net, GOBS can isolate the source of error by checking DFMs and constraint modules in a hierarchy of the net. Once error source is isolated, GOBS either recalibrate or replan the system based on the action net procedures.

3.1.2 GOBS "adaptive trenching" example.

The science objective in this case is to trench materials below the planetary surface, obtaining more pristine samples, viewing layered strata, making local measurements (e.g., temperature), etc. The soil properties are not well known in advance as to cohesion, variability, hidden obstacles, etc. A ground-station scientist specifies the desired trench location through selection of points on 2D image-plane data which has been downloaded from the lander-based stereo cameras. Once the selection is complete

and the desired robot trajectory is verified in terms of reachability, then trajectory data is uploaded to the GOBS architecture. Inverse kinematics of MarsArmII, or the rover-based MicroArm-1, are used to compute the joint configuration that achieves a given end-effector position as well as a given in-plane orientation. In general, once the desired end-effector location is known, the roll joint (theta(1)) is first computed. Once theta(1) is determined (cf. the earlier DH-parameters), the remainder of the arm can be considered a planar manipulator maneuvering in the "trenching plane." Then, given the end-effector tip position and orientation with respect to the trenching plane, the last three joint rotations (theta(2) - theta(4)) are calculated. A maneuver is executed, monitored, and adapted in position/forces in accordance with various sensor-based constraints, and an underlying discrete state task model for the trenching behavior. **Figure 6** below shows the science operator user interface for one such actual laboratory experiment with MarsArmII, as well as a computer simulation used to verify various aspects of GOBS architecture functionality

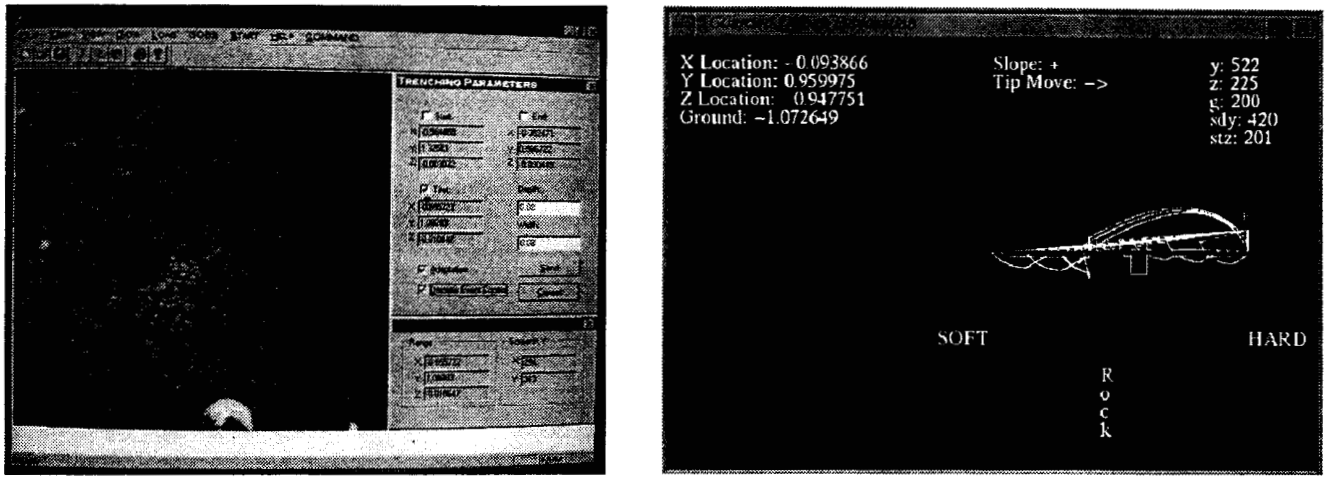

Figure 6. *At left*, screen display of terrain in front of lander, as viewed from a mast camera of Figure 1 (desired trench line has been identified per angled black cursor in image, and cross-hair start and end points); *right*, a simulation of GOBS trajectory generation during trenching, with force feedback/adaptive compliance to tip interactions with variable soil

A GOBS architecture lower level action net for soil trenching is shown in **Figure 7**, wherein actions are depicted by boxes and states are depicted by (double) circles. The lower level action net includes details of actions defined at a higher level. For this particular GOBS application, adaptive trenching is designed with four levels of control hierarchy (bottom to top) 1) PID control, 2) impedance control, 3) adaptive reference control, and 4) discrete event control. Impedance control implements a scoop compliance to cope with arm reactions from unknown soil properties. Adaptive reference control modifies the initial trenching trajectories by replanning according to actual trajectories observed under impedance control in reaction to actual soil properties. Discrete event control addresses extreme cases where the scoop encounters an abrupt change of environmental contact such as embedded rock. This control scheme for robotic trenching, *adaptive impedance control*, runs with a different intrinsic time scale at each level.

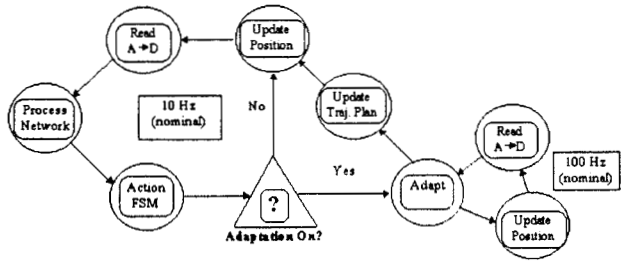

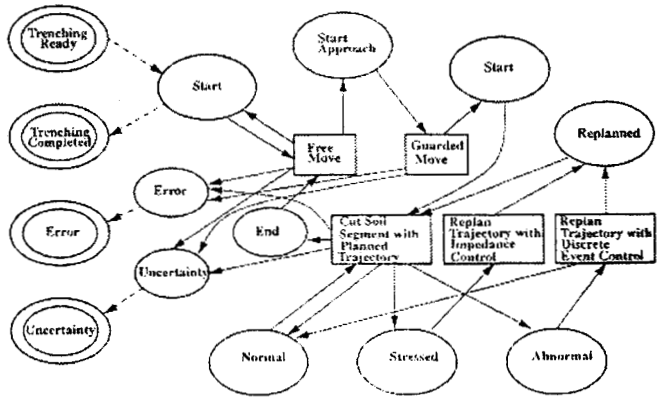

Figure 7. *At left*, a GOBS perception/action pseudo-control loop for adaptive trenching; *right*, a lower level action net implementing adaptive trenching behavior

In experimental implementation of the above adaptive trenching behavior, our baseline implementation is as follows:

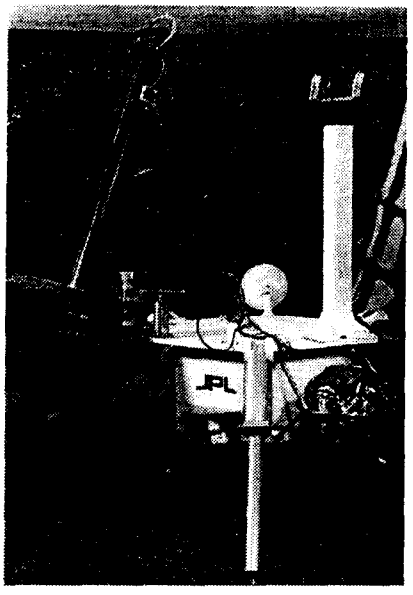

- arm is commanded, via designated trench line, to start position
- arm traces trajectory with a minimum force to estimate terrain
- arm makes vertical penetration move to estimate soil cohesion
- based on this mechanical resistance, a scoop compliance is set
- compliance is referenced to a defined rotational motion center
- a nominal *penetrate-sweep-pile* arm trajectory is commanded
- if the measured force stays in limit, a full trajectory is completed
- actual versus planned path is compared at sweep completion
- model reference trajectory is modified for the next iterate
- reflecting newly observed soil resistance of last layer sweep
- adaptation is implemented as change of scoop rotation center
- trajectory adaptation is guaranteed stable by heuristic limits
- if excessive resistance is encountered, a discrete action occurs
- a parking trajectory is executed with re-initiation of sweep
- Figure 6 illustrates the above via a stochastic simulation

3.1.3 Error recovery and the self-calibrating stereo concept

We sketch an example of error monitoring and recovery, to illustrate logical sensor interactions in the GOBS perception net, and to introduce self-calibrating stereo vision: An arm is commanded to a given Cartesian workspace point, which is either successfully reached or not in given time. Assume the arm does reach the desired position, an observable feature in the workspace. We compare position inferred from joint encoder readings to calibrated stereo localization of a 3D marker at the arm end. If readings agree within their modeled error bounds, then operation is deemed normal and perception net data fusion can proceed via DFM function of a logical sensor. If the sensor sources disagree, then one or both are biased. We can check the arm calibration by referencing arm encoders to a zero point, or similarly with a potentiometer and absolute joint position reference (An accurate underlying kinematics model is assumed, but note we have recently demonstrated a means of eye-to-hand calibration which does require this [ ]). Once arm calibration is verified, we then check for visual calibration bias, which if present, we address as below. In the latter case where the arm does reach it planned trajectory end point, but encoders and vision estimates agree, it is likely the controller or actuators are faulty. One might proceed by a joint-wise set of induced motions to isolate the error source/fault. In the event the encoder and visual estimates disagree, then the full range of encoder/actuator/vision calibration failure modes must be examined.

We are developing stereo self-calibration as decentralized sensor fusion [8, 19], implemented as perception-net based geometric data fusion and iterative parameter update [16]. The objective is on-line calibration of vision-based manipulation systems, examples being our lander and rover sampling arms. In analogy with the above example, we assume a sequence of measurements of the 3D position of a single feature point located at the manipulator end-effector by the stereo camera, as well as forward kinematics estimates of the manipulator through its encoders. Both measurements are assumed noisy and biased. The proposed perception-net based self-calibration algorithm then takes the noisy and biased readings from the stereo vision and manipulator and fuses them in real-time in a way that is defined by the net architecture. The net provides all possible spatial and temporal fusion components embedded in a hierarchy of data extracted through feature transformations as well as all possible constraints to be satisfied among the data. While the uncertainty involved in the 3D feature point is reduced through the process of data fusion and constraint satisfaction, the biases are exposed, detected, and estimated concurrently through iterative parameter update. The self-calibration system is thus composed of: 1) the algorithm for forward data propagation through feature transformation and data fusion, 2) the algorithm for backward error propagation through constraint satisfaction, 3) the algorithm for detecting the existence of biases, and 4) the algorithm of parameter update to remove existing biases. We have developed a software prototype for this procedure written in C (simulated in a PC environment) for application to MarsArm II and MicroArm-I based robotic sampling demonstration. We have evaluated the technique in simulation, including convergence properties as a function of bias and noise levels [16]. This is in essence a self-correcting system for modeling errors concurrently with state estimation. The proposed method is equivalently a generalized form of Kalman filter, featuring decentralized data fusion, with emphasis of the incorporation of system constraints, as well as the concurrent identification and correction of modeling errors in nonlinear system dynamics.

4. POWER OPTIMAL TRAJECTORY CONTROL

In this section we return to a more conventional topic in manipulator control. Our objective is to design a minimal power trajectory for moving a robot arm to accomplish a task objective. This is a practical problem for space applications, wherein sub-system power budgets are often very limited and overall system power resources may have a finite mission lifetime. In its generality -- reflecting the full regime of control synthesis in free-space and force contact modes -- this is a complicated and unsolved robotics problem [6, 7]. The more restricted case of generating time-constrained or torque-optimized trajectories is better understood and has been the subject of research for a good while.

Approaches for solving torque optimized trajectories include dynamic programming search in state space for point to point motion [31] and for motions along a specified path [27, 28], the application of the Hamilton-Jacobi-Bellman equation [14] or Pontryagin's minimum principle [18] to obtain optimal feedback laws for point to point motion and for overall motions along a specified path, and solution of two point boundary value problem with a time-energy cost function for motions along a specified path [26]. Each of these approaches, in spite of their merits, needs further improvement in one or more of the following areas:

- computability of high dimensional, coupled, nonlinear arm dynamics, especially without pre-specified path
- identifying realistic dynamic and kinematic constraints, e.g., joint torque, joint angle and velocity limits, etc.
- avoiding trapping in local minima (finding a global optimum over a non-convex solution space)
- generation of optimal trajectories under the consideration of arm flexibility and variable speeds
- on-line trajectory generation of optimized trajectories, including adaptation to variable tasks and payloads

Our design begins with development of the complete dynamical model of the arm in a symbolic form, taking into consideration not only the inertial force terms and gravity loading due to joint and link masses, but also the effects of Coulomb friction, viscous damping, actuator inertia, and gear efficiencies. We then formulate the problem of power optimized trajectory synthesis in terms of the optimal control of a nonlinear system (represented by the arm dynamic model) under inequality constraints on control (joint torques) and state (joint angles and velocities), where the cost function may be defined based on the trade-off between the power consumption and task execution time. We obtain such a simulated MarsArmI solution by implementing an iterative optimization method for solving the two point boundary value problem in Matlab codes. We show comparative results for optimized and non-optimized joint trajectories (angles $\underline{\mathbf{q}}$ and velocities $\underline{\mathbf{q}}'$) and joint torque histories (torques $\underline{\mathbf{u}}$) in **Figure 8** (below and overleaf)

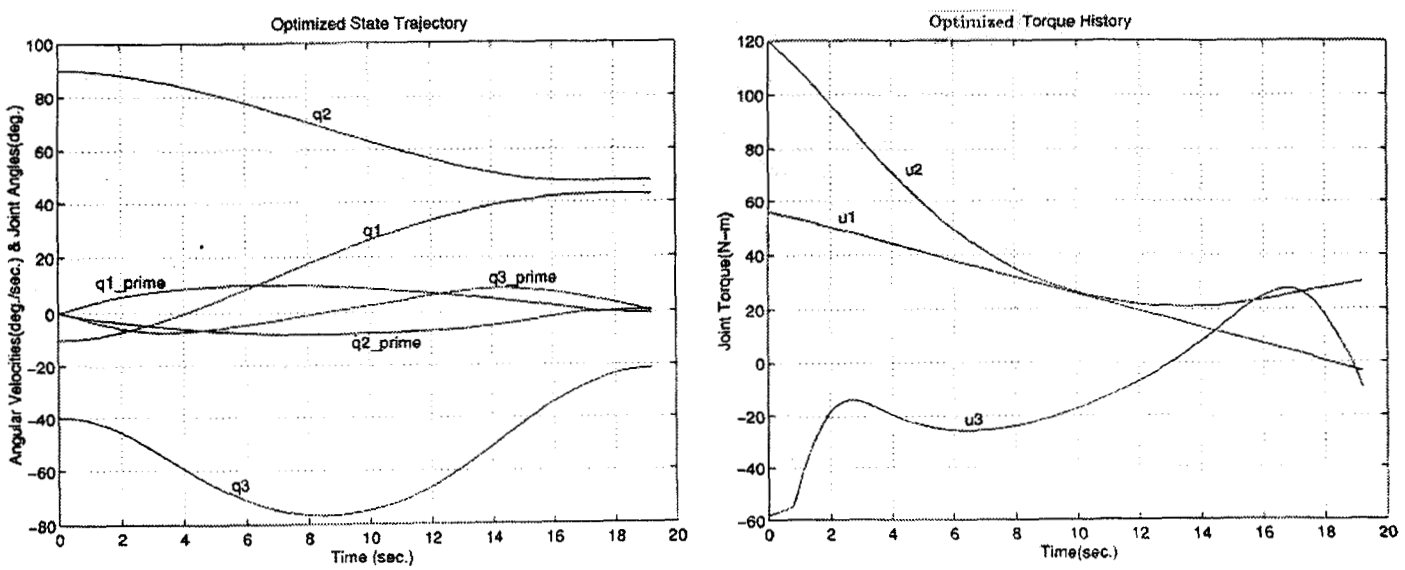

Figure 8. *Above*, power optimal joint kinematics and torque histories for MarsArmI performing a two point boundary free space manipulation; *below*, same, as computed from a conventional control based on linear trajectory with parabolic blend

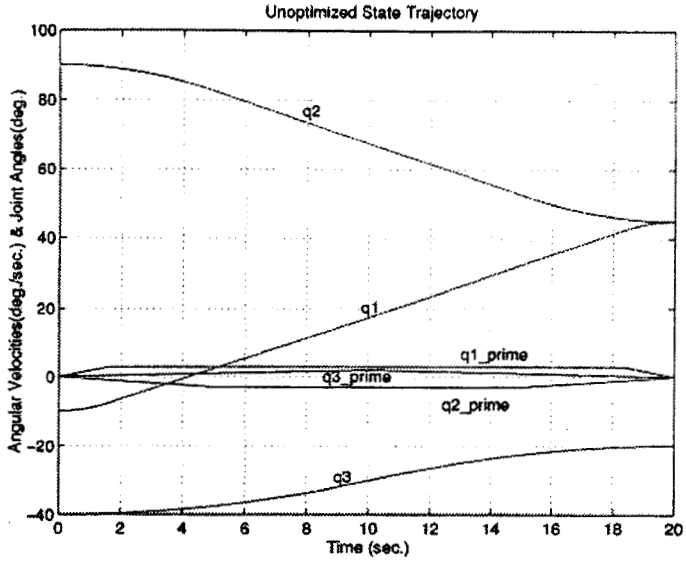

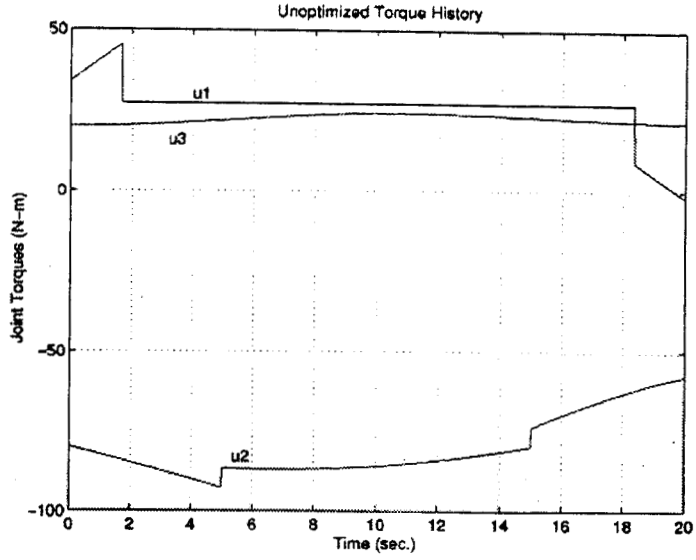

In simulation, we observe up to 40% power conservation with the optimizing trajectories by comparison to a conventional control non-optimizing control (linear function with parabolic blend). We have successfully executed these trajectories in MarsArmI (modeling system physical parameters as a mix of known and estimated quantities). For on-line synthesis, one might construct an approximating real-time feedback control law (using a linearized system dynamic model), coupled to adaptive compensation control for the nonlinear terms; or, one could generalize samples of reference trajectories with polynomial or neural network approximation for interpolation. We note there is an inherent space-time optimization trade-off introduced by arm tracking versus power compensation behaviors: Due to arm/joint flexion, arm control degrades at higher joint velocities. At low joint velocities, joint drive losses increase. The combined effect is not well understood, and infers a multi-parameter optimization in time and spatial variables of a given system. The practical importance of these issues to lander and rover sampling is unknown at present.

5. CONCLUSION

Continuing our earlier work on MarsArmI, we have established a further base of robot design and experimental experience toward higher dexterity, light robotic systems for planetary exploration. Highlights of this work, as demonstrated in simulated lander and rover scenarios, include new materials, mechanical designs, actuators, sensing techniques, and task-level dexterous controls for planetary sample acquisition, *in situ* analysis, and sample return processing of future Mars missions. Early results of this research provide the concept for NASA's forthcoming Mars Surveyor '98 robotic science mission. More recent advances reported here will support rover-based sampling and sample cache retrievals. While significant design concepts and experimental results have been obtained, many interesting, important questions remain open. These include: survivability of materials and components, genericity and performance of advanced controls, strategies and efficiency of robot arm use in hard media sampling, potential to integrate and effectively use miniature science instruments, impact of real-time space computing limitations, improved 3D sensing/navigation, and increased autonomy & computer intelligence [20].

ACKNOWLEDGEMENTS

This work was carried out at the Jet Propulsion Laboratory, California Institute of Technology, under a contract with the National Aeronautics and Space Administration. We gratefully acknowledge support of the NASA Telerobotics Program for this research. Areas of cognizance for the above reported work are: P. Schenker, PI; E. Baumgartner, system engineering; S. Lee, controls and 3D sensors; H. Aghazarian, software development & user interfaces; M. Garrett, electronics; R. Lindemann, mechanical design; K. Brown, composite engineering; Y. Bar-Cohen, advanced actuation. B. Hoffman carries out portions of the GOBS software and control implementation as a visiting student under the MIT-EIP cooperative study program. T. Huntsberger has contributed significantly to the cache localization problem during a NASA Summer Faculty Fellow visit with P. Schenker. E. Paljug and G. Tharp assisted simulations and experimental implementation of the power optimal trajectory work. S. Kim conducts cooperative science experiments on sampling and *in-situ* analysis, utilizing new miniature NASA NMR instrumentation of his design. D. Paige, UCLA, has provided valuable, continuing guidance toward robotics requirements for Mars science exploration.

REFERENCES

1. J. S. Albus, Brains, Behavior, and Robotics, McGraw-Hill, 1981, New York, NY.

2. J. S. Albus, R. Lumia, and H. McCain, "Hierarchical control of intelligent machines applied to Space Station robots," IEEE Trans. Aerospace and Electronic Systems, Vol. 24, No. 5, pp. 535-541, September, 1988.

3. J. S. Albus and R. Quintero, "Toward a reference model architecture for real-time intelligent control systems (ARTICS)," in Robotics and Manufacturing, Vol. 3 (Proc. ISRAM '90). ASME Press, 1990, New York, NY; and, D. Simon, B. Espiau, and K. Kapellos, "Computer-aided design of a generic robot controller handling reactivity and real-time control issues," IEEE Trans. Control Systems and Technology., Vol. 1, No. 4, December, 1993.

4. E. T. Baumgartner and P. S. Schenker, "Autonomous image-plane robot control for Martian lander operations," in Proc. 1996 IEEE Intl. Conf. Robotics and Automation , pp. 726-731, Minneapolis, MN, April; E. T. Baumgartner and N. A. Klymyshyn, "A sensitivity analysis for a remote vision-guided robot arm under imprecise supervisory control," in Sensor Fusion and Distributed Robotic Agents, Proc. SPIE 2905, Boston, MA, November, 1996.

5. L. Conway, R. Volz, and M. Walker, "Teleautonomous systems: methods and architectures for intermingling autonomous and telerobotic technology," in Proc. 1987 IEEE Intl. Conf. Robotics and Automation, Raleigh, NC, March; P. S. Schenker, "Intelligent robots for space applications," in Intelligent Robotic Systems: Analysis, Design, and Programming (S. Tzafestas, Ed.). Marcel Dekker, 1991: New York, NY, pp. 545-591; and, P. S. Schenker and G. T. McKee, "Man-machine interaction in telerobotic systems and issues in the architecture of intelligent and cooperative control," in Proc.IEEE/Intl. Symp. Intell Control Workshop (Architectures for Semiotic Modeling and Situation Analysis in Large Complex Systems, Orgs.: J. Albus, A. Meystel, D. Pospelov, T. Reader), 12 pp., Monterey, CA, August, 1995.

6. J. J. Craig, Introduction to Robotics: Mechanics and Control, Addison-Wesley, Reading, MA, 1989 (2nd. Ed); Tutorial on Robotics (Eds., C.S.G. Lee, R.C. Gonzales, and K.S. Fu). IEEE Computer Society Press, 1986 (2nd edition), Washington, D.C; and, The Robotics Review I (O. Khatib, J. Craig, and T. Lozano-Perez, Eds.), The MIT Press (McGraw-Hill), Cambridge, MA, 1989.

7. B. R. Donald, P. Xavier, J. Canny, and J. Reif, "Kinodynamic motion planning.," Journal of the ACM, Vol. 40, No. 5, pp. 1048-1066, November, 1993.

8. H. F. Durrant-Whyte, "Consistent integration and propagation of disparate sensor observations," Intl. Jrnl. Robotics Research, Vol. 6, No. 3, pp. 3-24, 1987.

9. "Geometric Uncertainty in Motion Planning: Summary Report and Bibliography (Eds., K. Y. Goldberg, M. T. Mason, and A. Requicha)," from NSF sponsored workshop, report issued as IRIS TR No. 297, University of Southern California, Los Angeles, CA August, 1992.

10. S. Hayati, R. Volpe, P. Backes, J. Balaram, R. Welch, R. Ivlev, G. Tharp, S. Peters, T. Ohm, R. Petras, and S. Laubach, "The Rocky 7 rover: a Mars sciencecraft prototype," Proc. 1997 Intl. IEEE Conf. on Robotics and Automation, Albuquerque, NM, April 20-25; and, P. G. Backes and G. Tharp, "The WEB interface for telescience (WITS)," ibid.; see also, R. Volpe, J. Balaram, T. Ohm, and R. Ivlev, "The Rocky 7 Mars rover prototype," Proc. IEEE/RSJ International Conf. on Intelligent Robots and Systems (IROS '96), Osaka, Japan, November 4-8, 1996, and citations therein.

11. T. Henderson and E. Shilcrat, "Logical sensor systems," Jrnl. Robotic Systems, Vol 1., No. 2, pp. 169-193, 1984; and, T. Henderson, C. Hansen, and B, Bhanu, "The specification of distributed sensing and control," Jrnl. Robotic Systems, Vol. 2, No. 4, pp. 387-396, 1985.

12. N. Hogan, "Impedance control: an approach to manipulation: part I - theory," ASME Jrnl. Dynamic Systems, Measurement, and Control, Vol. 107, pp. 1-7, 1985; N. Hogan and E. Colgate, "Stability problems in contact tasks," (and references therein), in The Robotics Review I (Eds., O. Khatib, J. Craig, and T. Lozano-Perez, Eds.), pp. 339-348, The MIT Press (McGraw-Hill), Cambridge, MA, 1989; and, R. Volpe, "Techniques for Collision Prevention, Impact Stability, and Force Control by Space Manipulators," in Teleoperation and Robotics in Space (Eds., S. Skaar and C. Ruoff), AAAI, Washington, D. C., 1994, pages 175-208.

13. B. K. P. Horn, Robot Vision, The MIT Press (McGraw-Hill), Cambridge, MA, 1986; and R. Y. Tsai, "A versatile camera calibration technique for high-accuracy 3D machine vision metrology using off-the-shelf TV cameras and lenses," IEEE Jrnl. Robotics and Automation, Vol. RA-3, 4, pp. 323-344, August 1987.

14. R. Johansson, "Quadratic optimization of motion coordination and control," IEEE Trans. on Automatic Control, Vol. 35, No. 11, pp. 1197-1208, 1990.

15. S. Lee and P. Schenker, "Autonomous synthesis of goal-oriented behaviors for planetary robotic sampling," in Sensor Fusion and Distributed Robotic Agents Conference, SPIE Proc. 2905, Boston, MA, Nov. 1996; S. Lee, B. Hoffman, E. Baumgartner, and P. Schenker, "GOBS: An intelligent system architecture for planetary robotic sampling," in Proc. Intl. Conf. on Advanced Robotics (ICAR'97), Monterey, CA, July, 1997.

16. S. Lee, "Sensor fusion and planning with perception and action network," in Proc. IEEE/SICE/RSJ Multi-Sensor Fusion and Integration for Intelligent Systems (MFI'96), Washington, DC., Dec. 1996; S. Lee, S. Ro, E. Baumgartner, and P. Schenker, "Self-calibration of eye-hand coordination system with decentralized data fusion," in Sensor Fusion and Decentralized Control in Autonomous Robotic Systems, SPIE Proc. 3209, Pittsburgh, PA, October, 1997.

17. S. Lee, S-C. Ahn, A. Meyyappan, and P. Schenker, "3D sensing based on hand-eye camera motions," in Sensor Fusion and Distributed Robotic Agents Conference, SPIE Proc. 2905, Boston, MA, Nov. 1996; S. Lee, S-C. Ahn, A. Meyyappan, and P. Schenker, "Experiment on depth from magnification and blurring," in Proc. 1997 IEEE/RSJ Intl. Conf. on Intelligent Robots and Systems (IROS'97), Grenoble, France, September.

18. P. Lu, "Minimum energy feedback control of robots," Proc. American Control Conference, pp. 2947-2951, 1992.

19. R. C. Luo and M. G. Kay, "Multisensor integration and fusion in intelligent systems," IEEE Trans. Systems, Man, and Cybernetics, Vol. 19, No. 5, pp. 901-931, October, 1989; K. A. Tarabanis, P. K. Allen, and R. Y. Tsai, "A survey of sensor planning in computer vision," IEEE Trans. Robotics and Automation, Vol. 11, No. 1, pp. 84-104, February, 1995.

20. Designing Autonomous Agents: Theory and Practice from Biology to Engineering and Back (P. Maes, Ed.), MIT Press, March 1991 (Also published as a special issue of the journal, "Robotics and Autonomous Systems," June 1990); and, Toward Learning Robots (Ed., W. Van de Welde). The MIT Press, 1993, Cambridge, MA.

21. L. Matthies et al., "Obstacle detection for unmanned ground vehicles: a progress report," Proc. 7th Intl. Symp. Robotics Research, Germany, October, 1996 (ref: Springer-Verlag, New York, NY, 1996, ISBN 3-540-76043-1); and, L. Matthies, C. Olson, G. Tharp, S. Laubach, "Visual localization methods for Mars rovers using lander, rover, and descent imagery," Intl. Symposium on Artificial Intelligence, Robotics, and Automation in Space (i-SAIRAS '97), Tokyo, Japan, July, 1997.

22. See *http://mvacs.ess.ucla.edu/*, D. A. Paige (PI, Integrated Science Payload), NASA-Mars Surveyor Program/Mars Volatiles and Climate Surveyor '98 (MVACS).

23. P. S. Schenker, D. L. Blaney, D. K. Brown, Y. Bar-Cohen, S-S. Lih, R. A. Lindemann, E. D. Paljug, J. T. Slostad, G. K. Tharp, C. E. Tucker, C. J. Voorhees, and C. Weisbin, Jet Propulsion Lab.; E. T. Baumgartner, Mich. Tech. Univ.; R. B. Singer, R. Reid, Univ. of Arizona, "Mars lander robotics and machine vision capabilities for *in situ* planetary science," in Intelligent Robots and Computer Vision XIV, SPIE Proc. 2588, Philadelphia, PA, October, 1995.

24. P. S. Schenker, Y. Bar-Cohen, D. K. Brown, R. A. Lindemann, M. S. Garrett, E. T. Baumgartner, S. Lee, S.-S. Lih and B. Joffe, "A composite manipulator utilizing rotary piezoelectric motors: new robotic technologies for Mars in-situ planetary science," in Enabling Technologies: Smart Structures and Integrated Systems, SPIE Proc. 3041, San Diego, CA, March, 1997.

25. P. S. Schenker, L. F. Sword, A. J. Ganino, D. B. Bickler, G. S. Hickey, D. K. Brown, E. T. Baumgartner, L. H. Matthies, B. H. Wilcox, T. Balch, H. Aghazarian, M. S. Garrett, "Lightweight rovers for Mars science exploration and sample return," in Intelligent Robots and Computer Vision XVI, SPIE Proc. 3208, Pittsburgh, PA, October, 1997.

26. Z. Shiller, "Time-energy optimal control of articulated systems with geometric path constraints," Proc. IEEE Conf. Decision and Control, 1994.

27. K. G. Shin and N. D. McKay, "A dynamic programming approach to trajectory planning of robot manipulators," IEEE Trans. On Automatic Control,, Vol. AC-31, No.6, pp. 491-500, 1986.

28. S. Singh and Leu, M.C., "Optimal trajectory generation for robot manipulators using dynamic programming," Journal of Dynamic Systems, Measurement, and Control, Vol. 109, pp. 88-96, June, 1987.

29. T. Ueha and Y. Tomikawa, *Ultrasonic Motors - Theory and Applications*, Oxford Science Publications, Oxford, England, 1993; also, J. Hollerbach, I. W. Hunter, and J. Ballantyne, "A comparative analysis of actuator technologies for robotics," in *Robotics Review 2 (eds. O. Khatib, J. Craig, and T. Lozano-Perez)*, The MIT Press, Cambridge, MA, 1992; JPL-specific developments are discussed in: Y. Bar-Cohen, S.-S. Lih and N. W. Hagood, "Solid-state actuation as a drive mechanism for miniature spacecraft," Proc. 9th Annual AIAA/USU Conf. on Small Satellites, Utah State University, Iowa, Sep 19-21, 1995; Y. Bar-Cohen, S.-S. Lih and N. W. Hagood, "Miniature ultrasonic rotary motors," Proc. AVS 2nd Micromachining Workshop, Anaheim, CA, September 19-21, 1995; S.-S. Lih and Y. Bar-Cohen "Rotary piezoelectric motors actuated by traveling waves," in Enabling Technologies: Smart Structures and Integrated Systems, SPIE Proc. 3041, San Diego, CA, March, 1997.

30. R. Volpe, T. Ohm, R. Petras, R. Welch, J. Balaram, R. Ivlev, "A prototype manipulation system for Mars rover science operations," Proc. IEEE/RSJ Intl. Conference on Intelligent Robots and Systems (IROS'97), Grenoble, France, September 7-11, 1997.

31. M. Vukobratovic and M. Kircanski, "A method for optimal synthesis of robot manipulator trajectories," Journal of Systems, Measurement, and Control, Vol. 104, pp.188-193, June, 1982.

32. C. R. Weisbin, D. Lavery, and G. Rodriguez, "Robotics technology for planetary missions into the 21st century," Proc. 1997 Intl. Conf. on Mobile Planetary Robots, Santa Monica, CA, January 29-31 (ref: Planetary Society, Pasadena, CA, Org: L. Friedman), and see also, http://robotics.jpl.nasa.gov, and link therein to Rover and Telerobotics Program Overview (Mars technologies); D. L. Shirley and J. R. Matijevic, "Mars rovers: past, present, and future," Proc. Princeton Space Studies Inst. 20th Anniversary Conf., May, 1997; and, The Rover Team [D. L. Shirley at al.], "The Pathfinder Microrover," Journal of Geophysical Research, Vol. 102, No. E2, pp. 3989-4001, Feb. 25, 1997; see also http://www.jpl.nasa.gov [ref: Mars Pathfinder Mission, Sojourner Rover].

33. Y. Yakimovsky and R. Cunningham, "A system for extracting three-dimensional measurements from a stereo pair of TV cameras," Computer Graphics and Image Processing, Vol. 7, pp. 195-210, 1978; D.. Gennery, "Stereo-camera calibration," Proc. DARPA Image Understanding Workshop, pp. 101-108, November, 1979; and, S. Ganapathy, "Decomposition of transformation matrices for robot vision," Proc. IEEE Intl. Conf. Robotics and Automation, pp. 130-139, 1984.